

Alma Mater Studiorum Università di Bologna
Archivio istituzionale della ricerca

Near-infrared hyperspectral imaging (NIR-HSI) and normalized difference image (NDI) data processing: An advanced method to map collagen in archaeological bones

This is the final peer-reviewed author's accepted manuscript (postprint) of the following publication:

Published Version:

Lugli, F., Sciutto, G., Oliveri, P., Malegori, C., Prati, S., Gatti, L., et al. (2021). Near-infrared hyperspectral imaging (NIR-HSI) and normalized difference image (NDI) data processing: An advanced method to map collagen in archaeological bones. TALANTA, 226, 1-7 [10.1016/j.talanta.2021.122126].

Availability:

This version is available at: <https://hdl.handle.net/11585/793752> since: 2021-02-08

Published:

DOI: <http://doi.org/10.1016/j.talanta.2021.122126>

Terms of use:

Some rights reserved. The terms and conditions for the reuse of this version of the manuscript are specified in the publishing policy. For all terms of use and more information see the publisher's website.

This item was downloaded from IRIS Università di Bologna (<https://cris.unibo.it/>).
When citing, please refer to the published version.

(Article begins on next page)

This is the final peer-reviewed accepted manuscript of:

Lugli, F., Sciutto, G., Oliveri, P., Malegori, C., Prati, S., Gatti, L., Silvestrini, S., Romandini, M., Catelli, E., Casale, M., Talamo, S., Iacumin, P., Benazzi, S., & Mazzeo, R. (2021). Near-infrared hyperspectral imaging (NIR-HSI) and normalized difference image (NDI) data processing: an advanced method to map collagen in archaeological bones. *Talanta* 226, 122126.

The final published version is available online at:
<https://doi.org/10.1016/j.talanta.2021.122126>

Rights / License:

The terms and conditions for the reuse of this version of the manuscript are specified in the publishing policy. For all terms of use and more information see the publisher's website.

This item was downloaded from IRIS Università di Bologna (<https://cris.unibo.it/>)

When citing, please refer to the published version.

Near-infrared hyperspectral imaging (NIR-HSI) and normalized difference image (NDI) data processing: an advanced method to map collagen in archaeological bones

F. Lugli¹, G. Sciutto^{2,*}, P. Oliveri^{3,*}, C. Malegori³, S. Prati², L. Gatti², S. Silvestrini¹, M. Romandini¹, E. Catelli², M. Casale³, S. Talamo^{4,5}, P. Iacumin⁶, S. Benazzi^{1,5}, R. Mazzeo²

¹ University of Bologna, Department of Cultural Heritage, Ravenna Campus, Via degli Ariani, 1 – 48121 Ravenna, Italy

² University of Bologna, Department of Chemistry “G. Ciamician”, Ravenna Campus, Via Guaccimanni, 42 – 48121 Ravenna, Italy

³ University of Genova, Department of Pharmacy, Viale Cembrano 4, I-16148, Genova, Italy

⁴ University of Bologna, Department of Chemistry “G. Ciamician”, Via Selmi, 2 – 40126 Bologna, Italy

⁵ Department of Human Evolution, Max Planck Institute for Evolutionary Anthropology, Leipzig, Germany.

⁶ University of Parma, Department of Chemistry, Life Sciences and Environmental Sustainability, Parco Area Delle Scienze, 11/a, Parma, Italy.

*Corresponding authors. E-mail: giorgia.sciutto@unibo.it; oliveri@difar.unige.it

Abstract

In the present study, an innovative and highly efficient near-infrared hyperspectral imaging (NIR-HSI) method is proposed to provide spectral maps able to reveal collagen distribution in large-size bones, also offering semi-quantitative estimations. A recently introduced method for the construction of chemical maps, based on Normalized Difference Images (NDI), is declined in an innovative approach, through the exploitation of the NDI values computed for each pixel of the hyperspectral image to localize collagen and to extract information on its content by a direct comparison with known reference samples. The developed approach addresses an urgent issue of the analytical chemistry applied to bioarcheology researches, which rely on well-preserved collagen in bones to obtain key information on chronology, paleoecology and taxonomy. Indeed, the high demand for large-sample datasets and the consequent application of a wide variety of destructive analytical methods led to the considerable destruction of precious bone samples. NIR-HSI pre-screening allows researchers to properly select the sampling points for subsequent specific analyses, to minimize costs and time and to preserve integrity of archaeological bones (which are available in a very limited amount), providing further opportunities to understand our past.

Keywords

Chemical mapping; Normalized difference images (NDI); Near-infrared spectroscopy;
Hyperspectral imaging; Ancient bones; Collagen.

1. Introduction

Well-preserved collagen in bone remains is of utmost importance for the evaluation of biology, evolution and ethology of ancient humans and animals. Indeed, bone collagen informs on the individual's history, including its lifestyle, death and behaviour. To unveil such key information, collagen has been targeted by isotopic analyses, i.e. diet [1-6], mobility [7-9] and chronology [10-14], and more recently by proteomics, i.e. phylogeny [15-18] and species identification [19-21]. Collagen, a triple-helix fibrous protein, is the major constituent of the bone organic matrix [22]. After burial, bone collagen is usually subjected to post-depositional modifications due to degradation and contamination processes induced by several factors such as temperature, the time elapsed, soil, pH, humidity and microbial activity [23, 24]. Most of the current analytical protocols (e.g. isotopic, radiocarbon and proteomic) require well-preserved collagen in terms of content and quality, to provide valuable information [18,19, 21]. Isotope and radiocarbon analyses require more than 1% by weight of well-preserved collagen to yield accurate data [25]. Genetic analyses rely on the persistence of DNA molecules, possibly linked to the residual presence of collagen in bone remains [26, 27]. Similarly, also ZooMS (Zooarchaeology by Mass Spectrometry) and paleo-proteomics need preserved collagen peptides for taxonomic discrimination [21].

Previous works suggested that bones may present micro-areas with variable organic content due to diagenetic alterations [28, 29]. For example, intra-bone subsampling recently revealed that drilled bulk samples collected in an area of a few centimetres may present different nitrogen contents and, consequently, a variable intra-sample collagen content [28].

In the last few decades, the uncontrolled application of destructive analytical methods, aimed at finding well-preserved collagen, led to the destruction of numerous precious bone samples. A recent comment published on Nature [30] drew the attention of researchers in the analytical and anthropological fields to this issue, admonishing the reckless management of the heritage of human and animal remains. More sustainable non-invasive analytical methods are now needed, as well as

systematic documentation, across laboratories, on ancient humans and related species remains and on the success rate of data recovery. Thus, the possibility to gather a suitable amount of well-preserved collagen from bone specimens is crucial to obtain robust results and, potentially, to enable the analysis of those samples with low-bulk collagen but presenting specific areas with higher content.

Recently, several efforts have been focused on the development of reliable non-destructive pre-screening methods for the detection of collagen in bone specimens and the evaluation of their state of conservation. Spectroscopic techniques — as e.g. Fourier-transform infrared (FTIR) [21], Raman [31, 32] and near-infrared (NIR) [33–35] — played a focal role, but the possibility of an extensive mapping of samples has not been explored yet. Indeed, up to now, spectroscopic techniques allowed researchers to perform only point analyses on the bone specimens, without the possibility to clearly understand the spatial distribution of collagen – a crucial issue in heterogeneous samples. A previous study reported on the use of a NIR camera, with a reduced spectral range (900–1700 nm), on small cross-sectioned samples, using spectral bands associated with hydroxyapatite (O-H vibration modes) [36] to evaluate the diagenetic status of skeletal remains in support of Sr isotopic analyses.

In the present study, an innovative and non-invasive near-infrared hyperspectral imaging (NIR-HSI) method was developed for the simultaneous detection and localization of collagen in ancient bones, exploiting the short-wave infrared (SWIR) range (1000–2500 nm). In more detail, a fast and straightforward protocol to generate false colour chemical maps of the collagen distribution was proposed, based on the calculation of normalized difference images (NDI). The NDI method has been recently proposed in the frame of forensic and environmental applications [37, 38]. In the present study, it was implemented with an approach that exploits the NDI values extracted from each pixel of the hyperspectral image and compares the computed median values among real and reference samples. These values are reported in the ordinate axis of the box and whisker plot to

support the comparison and the evaluation of data obtained; thus, the joint examination of reference bones and test samples led to estimate the collagen content in each sample and within its different areas, supporting the identification of proper sampling points. The NDI approach is efficient when the target analytes have distinctive absorptions in the spectrum and are present at a detectable concentration in the sample analysed. The effect of signal interferences such as baseline effects is minimised by the mathematical transform itself.

This approach can radically reduce the destruction rate of precious samples, thus increasing the number of bones that can be submitted to guided micro-destructive sampling. In addition, the rapid pre-screening of large bones may contribute to optimize the time and the budget dedicated to time- and cost-consuming analyses, such as radiocarbon, stable isotopes and proteomics, reducing the total number of specimens analysed and, thus, potentially leading to a drastic drop in average research costs in these fields.

The method was, at first, assessed on six faunal samples with previously determined collagen content used as reference samples and then tested on three bone samples, characterized by different chronological period and site of excavation. To validate the method, the test bones were sampled in areas with different collagen content and quantitative analysis was performed through an acid demineralization method and compared with the outcomes of NIR imaging.

2. Materials and Methods

2.1 Samples

The method was applied on six reference samples with known collagen content (sample ID: FB-A, FB-B, FB-C, FB-D, FB-E, FB-F; see Table 1). Afterwards, the method was also tested on real test samples characterized by different chronological period and site of excavation. In detail, a human femur (MV-F) and a coxal bone (MV-C) coming from an Iron Age Italian site (Monterenzio

Vecchio, Bologna, ca. 4th-3rd century BC) [39], and a fauna sample from a Middle-Upper Paleolithic Italian site, namely RB (Riparo del Broion, Vicenza, Veneto, Italy, ca. 45'000 years BP) [40].

2.2 Hyperspectral imaging

HSI-NIR data were acquired by a push-broom system composed by a SWIR3 hyperspectral camera working in the 1000–2500 nm spectral range, at 5.6 nm spectral resolution (Specim Ltd, Finland). The instrumental setting is characterized by three halogen lamps (35 W, 430 lm, 2900 K, each) as illumination sources and a horizontal line scanner (40 × 20 cm moving stage) on which samples are laid down. The system is controlled by the Lumo Scanner v. 2.6 software (Specim Ltd, Finland). Prior to each measurement, dark (closed shutter) and white (99% reflectance Spectralon® rod) images were automatically recorded and used to compute the spectral reflectance value (R) for each pixel and wavelength. For the acquisition, the scan parameters were set as follow: frame rate equal to 50.00 Hz and exposure time equal to 9.00 ms; manual focus was tuned before the scan. The collected image data were organized in a three-dimensional data matrix, often called hypercube or, alternatively, spectral cube. The first two dimensions of the 3D array are vertical and horizontal spatial coordinates (pixels), while the third dimension represents the wavelengths (spectral dimension).

2.3 NIR-HSI data analysis

Collagen distribution was obtained representing the normalized difference image (NDI) [37, 38]:

$$NDI = \frac{R_{\lambda h} - R_{\lambda c}}{R_{\lambda h}} \quad (1)$$

where $R_{\lambda h}$ is the reflectance value at 1959 nm, attributed to the O-H banding second overtone and O-H stretching combination band of hydroxyapatite, and $R_{\lambda c}$ is the reflectance value at 2195 nm, attributed to N-H bending second overtone and C=O stretching combination of collagen. Plotting the NDI values for each pixel in a scale where red represents the maximum values and blue the

minimum values, a false colour chemical map is obtained, which represents the distribution of collagen. Owing to their high signal-to-noise ratio, spectra were used for the data analysis as raw data without any pre-treatment [41].

Regions of interest (ROIs) at predominant red, green and blue colours were automatically selected by defining, respectively, three numerical selection ranges of the colour values of the pixels in the resulting NDI maps. For each of the three ROI, the average NIR spectrum was computed by averaging the subset of spectra corresponding to the selected pixels.

NDI values of each different sample were also visualized in a box-and-whisker plot, in which the central mark of each box indicates the median, and the bottom and top edges of the box indicate the 25th and 75th percentiles, respectively. The comparison of the NDI median values calculated for reference samples with the ones obtained for the test samples enabled the estimation of collagen content in the test samples.

2.3 Collagen extraction and quantification

Bone collagen was extracted from reference and test samples and quantified at the Stable Isotope Laboratory of the University of Parma (Italy), following the protocol described by [42]. In brief, ca. 200 mg of bone was demineralized with 0.5 M HCl until no effervescence was observed. The resulting collagen ‘pseudomorphs’ were then treated with NaOH and lyophilized. Finally, collagen yields were calculated as the percentage of the extracted collagen weight over the total weight of the original bone sample.

3. Results and Discussion

Collagen distributions were obtained calculating the normalized difference images (NDI) [37, 38], as reported in the Materials and Methods paragraph, using the reflectance value at 2195 nm of collagen (N-H bending second overtone and C=O stretching combination band) and of the band at

1959 nm of hydroxyapatite (O-H bending second overtone and O-H stretching combination band) [34]. For the reference samples (labelled as FB) with known collagen content, merged chemical maps were obtained combining each sample in a single portfolio image, in which the chromatic scale was defined considering the NDI values calculated for each pixel in all the samples (Fig. 1). The colours observed in the maps are related to the different relative content of collagen (pure red: highest content, green: intermediate content, pure blue: lowest content). Samples FB-A and FB-B, which correspond to the lowest collagen content (2.9% wt of collagen), exhibited a bluish-light green colour (Fig. 1). Samples with a mid-level collagen content FB-C, FB-D and FB-E (ranging between 8% and 15% wt) showed a greenish hue with some yellow and light blue areas (Fig. 1). FB-F (20% wt of collagen) was characterized by several red and yellow pixels (highest content, >20% wt), distributed mainly on the bottom part of the sample (Fig. 1b). However, it can be noted that, in the upper left part of the sample, the distribution of collagen presented several blue spots, indicating a noticeably lower concentration, with respect to the bottom part.

Each map can be range-scaled individually to enhance the colour contrast and, consequently, the visualization of differences in collagen distribution within a single sample. For FB-D, for instance, the map analysed was range-scaled individually, from the lowest (pure blue) to the highest NDI value (pure red), to visually enhance the intra-sample variability in collagen content (Fig. 1c and 1e). The strategy followed for data processing enabled the automatic extraction of the average spectra from the three areas identified. As expected, the diagnostic bands associated to the presence of collagen at 2060 nm (N-H stretching combination band), 2195 nm and at 2293 nm (C-H stretching and bending combination band) [32] increased according to the collagen content (lower in the blue areas, higher in the red ones). This means that, depending on the sampling point, the quantity of collagen extracted by destructive analytical procedures (as the demineralization) may be remarkably different [28].

Thus, NIR-HSI maps revealed a very heterogeneous collagen distribution, both at a macro- and at a micro-scale (pixel size = 500 μm). Such heterogeneity was observed in all the samples, pointing out an urgent issue in bioarchaeology researches regarding the need for non-destructive pre-screening methods to support the identification of the richest collagen areas for designing further examinations.

Analyses of the reference set of samples showed that the NIR-HSI results were coherent with the collagen extraction yield. In particular, the NDI median values tended to increase according to the average collagen content (Fig. 2). This enabled a quick comparison among different specimens to identify the most suitable area to be submitted to further investigations by means of destructive analytical methods.

For sample FB-F, with the highest collagen content (20% wt), the highest NDI median was obtained (0.29), with box boundaries (25th and 75th percentiles) at 0.25 and 0.33. The median NDI value of sample FB-E (15% wt) was 0.27, with box boundaries at 0.24 and 0.29. FB-D (8.5% wt) and FB-C (8% wt) showed a similar median value, at around 0.26, with box boundaries at 0.23-0.29 for FB-D and at 0.24-0.29 for FB-C, exhibiting a partial box overlapping even with sample FB-E. Samples FB-A and FB-B, with the lowest amount of collagen (2.9% wt for both), showed a median NDI value at 0.22 and 0.23, respectively (with boundaries at 0.21 and 0.24 for FB-A, and at 0.21 and 0.25 for FB-B).

The distribution of the NDI values for each sample reported in the box and whisker plot (Fig. 2) showed that the median NDI values were positively correlated with the collagen content and that they increased according to the yield of the extracted collagen. These outcomes indicate the potential of NIR-HSI as a rapid tool to compare different bone remains to select the most interesting pieces and the most appropriate areas for the collection of micro-samples to be submitted to destructive analyses.

To further demonstrate the feasibility of NIR-HSI in the selection of sampling areas, three test samples (RB, MV-F, MV-C), with unknown collagen content were, at first, not-invasively mapped and, then, sampled in different points according to the collagen distributions obtained. The NDI merged map showed an evident heterogeneity, in terms of both collagen content and distribution (Fig. 3). RB, dating back to the Middle-Upper Palaeolithic (ca. 45 ka), resulted in be the samples with the lowest content, reflecting a post-depositional loss of organic matrix. The distribution of collagen content in this latter specimen was highly heterogeneous, as suggested by the presence of a large dark blue area with some green-yellowish spots, mainly present in a half of the sample. Conversely, the number of red and yellow pixels in the MV-F sample (4th-3rd cent BC) was remarkably elevate and widely distributed, indicating a higher collagen content localized in specific areas. MV-C (4th-3rd cent BC) showed a predominant green-yellowish tonality, in which some light blue and red areas were clearly identified. The highlighted intra-sample variability may be related to several factors as, e.g.: 1) diagenetic alterations [22]; 2) physiological differences in collagen density due to age [43]; 3) bio-mechanical properties of bone [44, 45].

Test samples were analysed to compare collagen distributions obtained with NIR-HSI with quantitative determinations of specific areas. Accordingly, in the box and whisker plot, the MV-F bone presented the highest NDI median value (0.32, with box boundaries equal to 0.28 and 0.36), while the median NDI values of MV-C was of 0.27, with box boundaries at 0.24 and 0.30. RB showed a high variability of the NDI values with a median of 0.20 (the lowest median value in all the samples analysed) and box boundaries at 0.14 and 0.26, suggesting a very heterogeneous collagen distribution.

The relative distributions of collagen deduced by examination of the NDI were confirmed by the quantitative determination in selected areas of samples MV-F, MV-C and RB, using HCl demineralization. Sample taken from the areas characterized by a high NDI value in MV-F (Fig. 3a and 3b) showed a higher collagen content (25% wt) than what was observed in the sample taken

from the areas with low NDI value of the same sample (12.5% wt of collagen), confirming the heterogeneity of collagen distribution in the femur. The same behaviour was observed in MV-C, where the collagen content was highly superior in the areas presenting a high NDI value (26.4% wt of collagen) with respect to ones with low NDI value (5.3% wt of collagen). A fragment taken from the area richest in collagen (high NDI value area) of sample RB showed a value of collagen of about 8.7% (wt). Interestingly, the maximum NDI value of RB, equal to 0.25 (Fig. 2), is of the same order of magnitude of the median value of samples FB-C and FB-D which contain a similar percentage of collagen.

These outcomes agree with the collagen yield of human bones from other Italian Metal-Age sites [46], reaching up ~30% wt. The coxal bone (sample MV-C) seemed characterized by an averagely lower collagen content with respect to MV-F, with collagen mostly localized in the exposed trabecular portion and part of the ilium. Due to the different remodelling rate between cortical and trabecular bone, an inter-tissue variability was expected [47]. Hence, higher collagen yield in the trabecular bone might be explained as relatively lower mineral content, if compared to the highly-mineralized cortical tissue [47, 48]. The Middle-Upper Paleolithic bone from Riparo Broion (RB) showed, as expected, a relatively low collagen yield, as observed by NIR imaging and collagen quantification (by performing acid demineralization). This may have been determined by the old age of the sample RB and by a strong post-depositional loss of organic matter, probably due to the combination of microbial attack and collagen hydrolysis [24].

4. Conclusions

The new NIR-HSI method developed provided an efficient mapping of collagen distribution, enabling an intra- and inter-sample comparison, fully exploiting the potentialities of the NDI data processing translated into chemical maps or into box and whisker plots, leading to a qualitative and semi-quantitative evaluation of the relative collagen content distribution.

Being fast and completely non-invasive, the NIR-HSI approach may help bone pre-screening, to identify interesting areas within the same specimen on which to drive subsequent targeted analyses, reducing size and number of samples, ultimately contributing to save money, time and to preserve bone integrity. Findings of the present study demonstrate that the high collagen content in old bones may be often restricted to a few areas, clearly indicating the importance of an adequate screening method to avoid incorrect evaluations and to maximize the ratio between information gain and sample destruction.

Based on the results showed here, further researches are now in progress to develop linear and non-linear multivariate regression models to extract quantitative data from the NIR-HSI chemical images.

Acknowledgments

FL, SS, MR and SB are supported by the European Research Council (ERC) under the European Union's Horizon 2020 research and innovation programme (grant agreement No 724046 – SUCCESS, <http://www.erc-success.eu/>) and the FARE programme 2018 (FARE Ricerca in Italia: Framework per l'attrazione e il rafforzamento delle eccellenze - MIUR). ST is supported by the European Research Council under the European Union's Horizon 2020 Research and Innovation Programme (grant agreement No. 803147 RESOLUTION, <https://site.unibo.it/resolution-erc/en>). The authors thank the “L. Fantini” Civic Archaeological Museum, Bologna Superintendency SABAP-BO, Veneto Archaeological Superintendency SAPAB and Friuli Venezia Giulia Superintendency for proving access to the skeletal materials. Two anonymous referees are thanked for their useful suggestions.

References

- [1] M. J. DeNiro, S. Epstein, Influence of diet on the distribution of nitrogen isotopes in animals, *Geochim. Cosmochim. Acta* 45(3) (1981) 341-351, [https://doi.org/10.1016/0016-7037\(81\)90244-1](https://doi.org/10.1016/0016-7037(81)90244-1).

- [2] M. J. Schoeninger, M. J., M. J. DeNiro, Nitrogen and carbon isotopic composition of bone collagen from marine and terrestrial animals, *Geochim. Cosmochim. Acta* 48(4) (1984) 625-639, [https://doi.org/10.1016/0016-7037\(84\)90091-7](https://doi.org/10.1016/0016-7037(84)90091-7).
- [3] M. P. Richards, P.B. Pettitt, E. Trinkaus, F.H. Smith, M. Paunović, I. Karavanić, Neanderthal diet at Vindija and Neanderthal predation: the evidence from stable isotopes, *Proc. Natl. Acad. Sci. USA* 97(13) (2000) 7663-7666, <https://doi.org/10.1073/pnas.120178997>.
- [4] H. Bocherens, D. Drucker, Trophic level isotopic enrichment of carbon and nitrogen in bone collagen: case studies from recent and ancient terrestrial ecosystems, *Int. J. Osteoarchaeol.* 13 (2003) 46-53, <https://doi.org/10.1002/oa.662>.
- [5] F. Lugli, A. Cipriani, G. Capecchi, S. Ricci, F. Boschini, P. Boscato, P. Iacumin, F. Badino, M. A. Mannino, S. Talamo, M. P. Richards, S. Benazzi, A. Ronchitelli, Strontium and stable isotope evidence of human mobility strategies across the Last Glacial Maximum in southern Italy, *Nat. Ecol. Evol.* 3 (2019) 905–911, <https://doi.org/10.1038/s41559-019-0900-8>.
- [6] K. Jaouen, M.P. Richards, A. Le Cabec, F. Welker, W. Rendu, J.-J. Hublin, S. Talamo, Exceptionally high $\delta^{15}\text{N}$ values in collagen single amino acids confirm Neandertals as high-trophic level carnivores, *Proc. Natl. Acad. Sci. USA* 116(11) (2019) 4928-4933, <https://doi.org/10.1073/pnas.1814087116>.
- [7] M. P. Richards, B.T. Fuller, R. E. Hedges, Sulphur isotopic variation in ancient bone collagen from Europe: implications for human palaeodiet, residence mobility, and modern pollutant studies, *Earth Planet. Sci. Lett.* 191(3-4) (2001) 185-190, [https://doi.org/10.1016/S0012-821X\(01\)00427-7](https://doi.org/10.1016/S0012-821X(01)00427-7).
- [8] O. Nehlich, The application of sulphur isotope analyses in archaeological research: a review, *Earth Sci. Rev.* 142 (2015) 1-17, <https://doi.org/10.1016/j.earscirev.2014.12.002>.
- [9] C. Wißing, H. Rougier, C. Baumann, A. Comeyne, I. Crevecoeur, D. G. Drucker, S. Gaudzinski-Windheuser, M. Germonpré, A. Gómez-Olivencia, J. Krause, T. Matthies, Y. I. Naito,

C. Posth, P. Semal, M. Street, H. Bocherens, Stable isotopes reveal patterns of diet and mobility in the last Neandertals and first modern humans in Europe, *Sci. Rep.* 9 (2019) 4433, <https://doi.org/10.1038/s41598-019-41033-3>.

[10] R. Longin, New method of collagen extraction for radiocarbon dating, *Nature* 230 (1971) 241-242, <https://doi.org/10.1038/230241a0>.

[11] T. F. G. Higham, R. M. Jacobi, C. Bronk Ramsey, AMS radiocarbon dating of ancient bone using ultrafiltration, *Radiocarbon* 48(2) (2006) 179-195, <https://doi.org/10.1017/S0033822200066388>.

[12] J. S. O. McCullagh, A. Marom, R. E. M. Hedges, Radiocarbon dating of individual amino acids from archaeological bone collagen, *Radiocarbon* 52(2) (2010) 620-634, <https://doi.org/10.1017/S0033822200045653>.

[13] S. Talamo, M. Hajdinjak, M. A. Mannino, L. Fasani, F. Welker, F. Martini, F. Romagnoli, R. Zorzin, M. Meyer, J. J. Hublin, Direct radiocarbon dating and genetic analyses on the purported Neanderthal mandible from the Monti Lessini (Italy), *Sci. Rep.* 6 (2016) 29144, <https://doi.org/10.1038/srep29144>.

[14] H. Fewlass, S. Talamo, L. Wacker, B. Kromer, T. Tuna, Y. Fagault, Y. E. Bard, S. P. McPherron, V. Aldeias, R. Maria, N.L. Martisius, L. Paskulin, Z. Rezek, V. Sinet-Mathiot, S. Sirakova, G. M. Smith, R. Spasov, F. Welker, N. Sirakov, T. Tsanova, J.-J. Hublin, A ^{14}C chronology for the Middle to Upper Palaeolithic transition at Bacho Kiro Cave, Bulgaria, *Nat. Ecol. Evol.* 4 (2020) 794–801, <https://doi.org/10.1038/s41559-020-1136-3>.

[15] J. M. Asara, M. H. Schweitzer, L. Freimark, M. Phillips, L. C. Cantley, Protein sequences from mastodon and *Tyrannosaurus rex* revealed by mass spectrometry, *Science* 316(5822) (2007) 280-285, <https://doi.org/10.1126/science.1137614>.

- [16] M. Buckley, A. Walker, S. Y. W. Ho, Y. Yang, C. Smith, P. Ashton, J. Thomas-Oates, E. Cappellini, H. Koon, K. Penkman, B. Elsworth, D. Ashford, C. Solazzo, P. Andrews, J. Strahler, B. Shapiro, P. Ostrom, H. Gandhi, W. Miller, B. Raney, M. I. Zylber, M. T. P. Gilbert, R. V. Prigodich, M. Ryan, K. F. Rijdsdijk, A. Janoo, M. J. Collins, Comment on "Protein Sequences from Mastodon and Tyrannosaurus rex Revealed by Mass Spectrometry", *Science* 319 (5859) (2008) 33, <https://doi.org/10.1126/science.1147046>.
- [17] M. Buckley, A Molecular Phylogeny of Plesiorcycteropus Reassigns the Extinct Mammalian Order 'Bibymalagasia', *PloS one* 8(3) (2013) e59614, <https://doi.org/10.1371/journal.pone.0059614>.
- [18] F. Welker, M. Hajdinjak, S. Talamo, K. Jaouen, M. Dannemann, F. David, M. Julien, M. Meyer, J. Kelso, I. Barnes, S. Brace, P. Kamminga, R. Fischer, B. M. Kessler, J. R. Stewart, S. Pääbo, M. J. Collins, J. J. Hublin, Palaeoproteomic evidence identifies archaic hominins associated with the Châtelperronian at the Grotte du Renne, *Proc. Natl. Acad. Sci. U. S. A.* 113 (2016) 11162-11167, <https://doi.org/10.1073/pnas.1605834113>.
- [19] M. Buckley, M. Collins, J. Thomas-Oates, J. C. Wilson, Species identification by analysis of bone collagen using matrix-assisted laser desorption/ionisation time-of-flight mass spectrometry, *Rapid Commun. Mass Spectrom.* 23 (2009) 3843–3854, <https://doi.org/10.1002/rcm.4316>.
- [20] S. Brown, T. Higham, V. Slon, S. Pääbo, M. Meyer, K. Douka, F. Brock, D. Comeskey, N. Procopio, M. Shunkov, A. Derevianko, M. Buckley, Identification of a new hominin bone from Denisova Cave, Siberia using collagen fingerprinting and mitochondrial DNA analysis, *Sci. Rep.* 6 (2016) 23559, <https://doi.org/10.1038/srep23559>.
- [21] G. Pothier Bouchard, S. M. Mentzer, J. Riel-Salvatore, J. Hodgkins, C. E. Miller, F. Negrino, R. Wogelius, M. Buckley, Portable FTIR for on-site screening of archaeological bone intended for

ZooMS collagen fingerprint analysis, *J. Archaeol. Sci. Rep.* 26 (2019) 101862, <https://doi.org/10.1016/j.jasrep.2019.05.027>.

[22] C. Kendall, A. M. H. Eriksen, I. Kontopoulos, M. J. Collins, G. Turner-Walker, Diagenesis of archaeological bone and tooth, *Palaeogeogr. Palaeoclimatol. Palaeoecol.* 491 (2018) 21-37, <https://doi.org/10.1016/j.palaeo.2017.11.041>.

[23] C. M. Nielsen-Marsh, R. E. Hedges, Patterns of diagenesis in bone I: the effects of site environments. *J. Archaeol. Sci.* 27(12) (2000) 1139-1150, <https://doi.org/10.1006/jasc.1999.0537>.

[24] R. E. M. Hedges, Bone diagenesis: an overview of processes, *Archaeometry* 44 (2002) 319–328, <https://doi.org/10.1111/1475-4754.00064>.

[25] G. J. van Klinken, Bone Collagen Quality Indicators for Palaeodietary and Radiocarbon Measurement, *J. Archaeol. Sci.* 26 (1999) 687–695, <https://doi.org/10.1006/jasc.1998.0385>.

[26] P. F. Campos, O. E. Craig, G. Turner-Walker, E. Peacock, E. Willerslev, M. T. P. Gilbert, DNA in ancient bone - Where is it located and how should we extract it?, *Ann. Anat.* 194 (2012) 7–16, <https://doi.org/10.1016/j.aanat.2011.07.003>.

[27] P. Korlević, S. Talamo, M. Meyer, A combined method for DNA analysis and radiocarbon dating from a single sample, *Sci. Rep.* 8 (2018) 4127, <https://doi.org/10.1038/s41598-018-22472-w>.

[28] E. Jacob, D. Querci, M. Caparros, C. Barroso Ruiz, T. Higham, T. Devière, Nitrogen content variation in archaeological bone and its implications for stable isotope analysis and radiocarbon dating, *J. Archaeol. Sci.* 93 (2018) 68-73, <https://doi.org/10.1016/j.jas.2018.02.019>.

[29] J. Anné, N. P. Edwards, F. Brigidi, P. Gueriau, V. L. Harvey, K. Geraki, L. Slimak, M. Buckley, R. A. Wogelius, Advances in bone preservation: Identifying possible collagen preservation using sulfur speciation mapping, *Palaeogeogr. Palaeoclimatol. Palaeoecol.* 520 (2019) 181-187, <https://doi.org/10.1016/j.palaeo.2019.01.030>.

- [30] K. Fox, J. Hawks, Use ancient remains more wisely, *Nature* 572 (2019) 581–583, <https://doi.org/10.1038/d41586-019-02516-5>.
- [31] C. A. M. France, D. B. Thomas, C. R. Doney, O. Madden, FT-Raman spectroscopy as a method for screening collagen diagenesis in bone, *J. Archaeol. Sci.* 42 (2014) 346–355, <https://doi.org/10.1016/j.jas.2013.11.020>.
- [32] O. Madden, D. M. W. Chan, M. Dundon, C. A. M. France, Quantifying collagen quality in archaeological bone: Improving data accuracy with benchtop and handheld Raman spectrometers, *J. Archaeol. Sci. Rep.* 18 (2018) 596–605, <https://doi.org/10.1016/j.jasrep.2017.11.034>.
- [33] D. Vincke, R. Miller, É. Stassart, M. Otte, P. Dardenne, M. Collins, K. Wilkinson, J. Stewart, V. Baeten, J. A. Fernández Pierna, Analysis of collagen preservation in bones recovered in archaeological contexts using NIR Hyperspectral Imaging, *Talanta* 18 (2014) 596–605, <https://doi.org/10.1016/j.talanta.2014.02.044>.
- [34] M. Sponheimer, C. M. Ryder, H. Fewlass, E. K. Smith, W. J. Pestle, S. Talamo, Saving Old Bones: a non-destructive method for bone collagen prescreening, *Sci. Rep.* 9 (2019) 13928, <https://doi.org/10.1038/s41598-019-50443-2>.
- [35] E. Catelli, G. Sciutto, S. Prati, M. V. Chavez Lozano, L. Gatti, F. Lugli, S. Silvestrini, S. Benazzi, E. Genorini, R. Mazzeo, A new miniaturised short-wave infrared (SWIR) spectrometer for on-site cultural heritage investigations, *Talanta* 218 (2020) 121112, <https://doi.org/10.1016/j.talanta.2020.121112>.
- [36] A. Retzmann, M. Blanz, A. Zitek, J. Irrgeher, J. Feldmann, M. Teschler-Nicola, T. Prohaska, A combined chemical imaging approach using (MC) LA-ICP-MS and NIR-HSI to evaluate the diagenetic status of bone material for Sr isotope analysis, *Anal. Bioanal. Chem.* 411 (2019) 565–580, <https://doi.org/10.1007/s00216-018-1489-5>.

- [37] C. Malegori, E. Alladio, P. Oliveri, C. Manis, M. Vincenti, P. Garofano, F. Barni, A. Berti, Identification of invisible biological traces in forensic evidences by hyperspectral NIR imaging combined with chemometrics, *Talanta* 215 (2020) 120911, <https://doi.org/10.1016/j.talanta.2020.120911>.
- [38] S. Piarulli, G. Sciutto, P. Oliveri, C. Malegori, S. Prati, R. Mazzeo, L. Airoidi, Chemosphere Rapid and direct detection of small microplastics in aquatic samples by a new near infrared hyperspectral imaging (NIR-HSI) method, *Chemosphere* 260 (2020) 127655, <https://doi.org/10.1016/j.chemosphere.2020.127655>.
- [39] R. Sorrentino, E. Bortolini, F. Lugli, G. Mancuso, L. Buti, G. Oxilia, A. Vazzana, C. Figus, M. C. Serrangeli, C. Margherita, A. Penzo, G. Gruppioni, A. Gottarelli, K. P. Jochum, M. G. Belcastro, A. Cipriani, R. N. M. Feeney, S. Benazzi, Unravelling biocultural population structure in 4th/3rd century BC Monterenzio Vecchio (Bologna, Italy) through a comparative analysis of strontium isotopes, non-metric dental evidence, and funerary practices, *PLoS One*. 13 (2018) e0193796, <https://doi.org/10.1371/journal.pone.0193796>.
- [40] M. Romandini, G. Oxilia, E. Bortolini, S. Peyrégne, D. Delpiano, A. Nava, D. Panetta, G. Di Domenico, P. Martini, S. Arrighi, F. Badino, C. Figus, F. Lugli, G. Marciani, S. Silvestrini, J. Sartorio, G. Terlato, J. Hublin, M. Meyer, L. Bondioli, T. Higham, V. Slon, M. Peresani, S. Benazzi, A late Neanderthal tooth from northeastern Italy, *J. Hum. Evol.* 147 (2020) 102867, <https://doi.org/10.1016/j.jhevol.2020.102867>.
- [41] P. Oliveri, C. Malegori, R. Simonetti, M. Casale, The impact of signal pre-processing on the final interpretation of analytical outcomes – A tutorial, *Anal. Chim. Acta*. 1058 (2019) 9–17, <https://doi.org/10.1016/j.aca.2018.10.055>.
- [42] S. H. Ambrose, Preparation and Characterization of Bone and Tooth Collagen for Isotopic Analysis, *J. Archaeol. Sci.* 17 (1990) 431–451, [https://doi.org/10.1016/0305-4403\(90\)90007-R](https://doi.org/10.1016/0305-4403(90)90007-R).

- [43] X. Wang, X. Shen, X. Li, C. Mauli Agrawal, Age-related changes in the collagen network and toughness of bone, *Bone* 31 (2002) 1-7, [https://doi.org/10.1016/S8756-3282\(01\)00697-4](https://doi.org/10.1016/S8756-3282(01)00697-4).
- [44] A. L. Boskey, T. M. Wright, R. D. Blank, Collagen and bone strength, *J. Bone Miner. Res.* 14 (1999) 330-335, <https://doi.org/10.1359/jbmr.1999.14.3.330>.
- [45] J. P. Spalazzi, A. L. Boskey, N. Pleshko, H. H. Lu, Quantitative Mapping of Matrix Content and Distribution across the Ligament-to-Bone Insertion, *PLoS One.* 8 (2013) e74349, <https://doi.org/10.1371/journal.pone.0074349>.
- [46] M. A. Tafuri, O. E. Craig, A. Canci, Stable isotope evidence for the consumption of millet and other plants in bronze age Italy, *Am. J. Phys. Anthropol.* 139 (2009) 146–153, <https://doi.org/10.1002/ajpa.20955>.
- [47] A. L. Boskey, R. Coleman, Aging and bone, *J. Dent. Res.* 89 (2010) 1333–1348, <https://doi.org/10.1177/0022034510377791>.
- [48] P. Pietschmann, M. Skalicky, M. Kneissel, M. Rauner, G. Hofbauer, D. Stupphann, A. Viidik, Bone structure and metabolism in a rodent model of male senile osteoporosis, *Exp. Gerontol.* 42 (2007) 1099–1108, <https://doi.org/10.1016/j.exger.2007.08.008>.

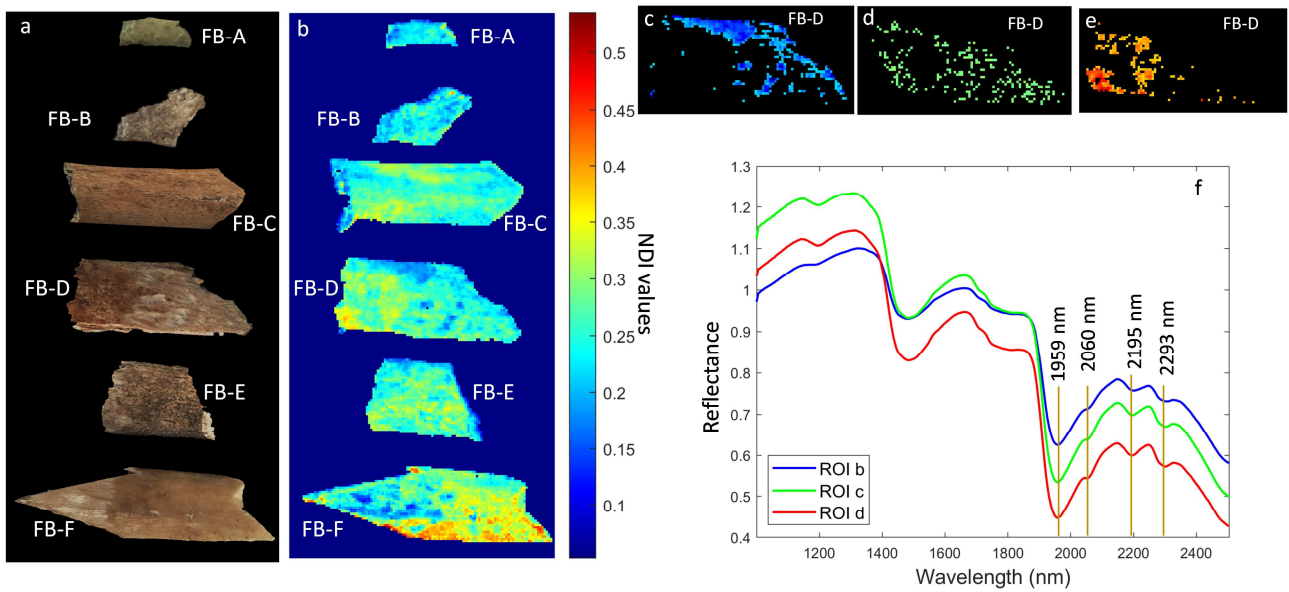


Figure 1. NIR-HSI results on reference samples. a) Photographs of the reference samples; b) NDI merged image of reference samples (from the above): FB-A, FB-B, FB-C, FB-D, FB-E, FB-F; c, d,e) ROIs referred to areas with different collagen content (blue: low, green: mid-level, red: high) in sample FB-D individually-scaled map; f) extracted averaged spectra from each ROI identified; diagnostic bands attributed to collagen (2060 nm: N-H stretching combination band; 2195 nm: N-H bending second overtone and C=O stretching combination 2293 nm: C-H stretching and bending combination band) and to hydroxyapatite (1959 nm: O-H banding second overtone and O-H stretching combination band) are marked in the plot.

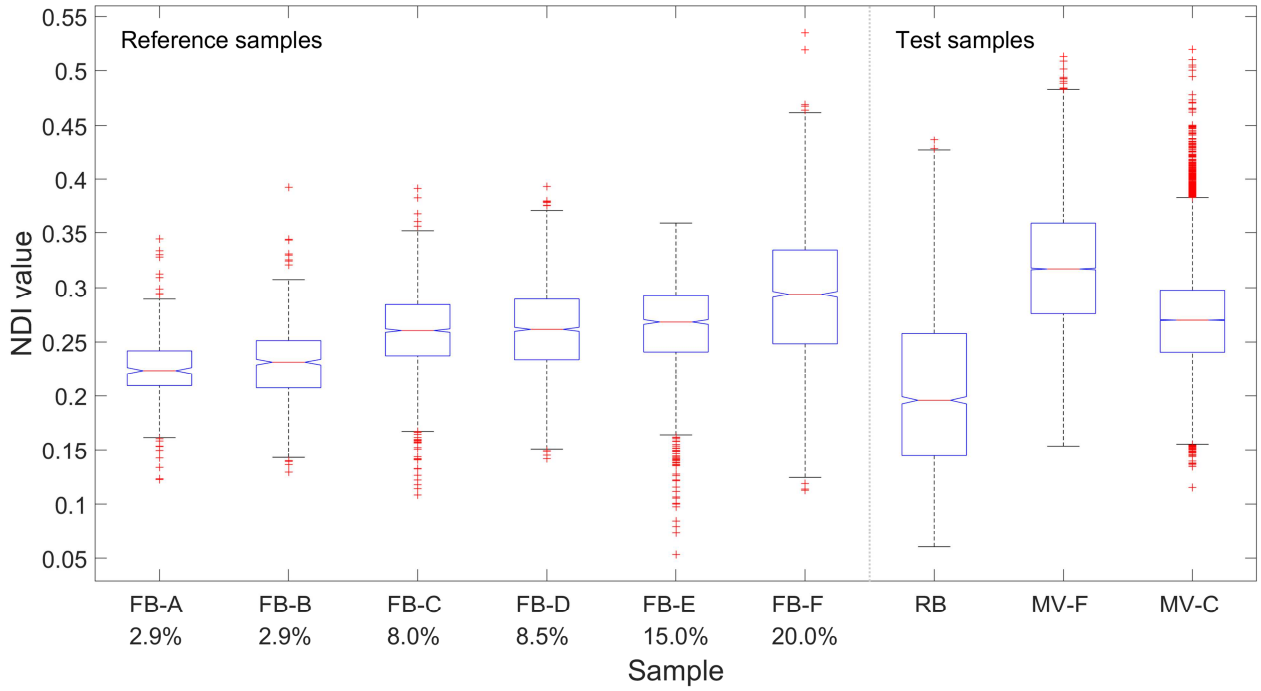


Figure 2. Box-and-whisker plot with NDI values. Box-and-whisker plot reporting the NDI values of reference (left) and test samples (right). Collagen yield obtained by acid demineralization is also reported for reference samples. On each box, the central red mark indicates the median, and the bottom and top blue edges of the box indicate the 25th and 75th percentiles, respectively. The black whiskers extend to the most extreme data points not considered as outliers, and outliers are plotted individually using the '+' red symbol. Number of pixels for each sample: FB-A: 312; FB-B: 693; FB-C: 2116; FB-D: 2226; FB-E: 1379; FB-F: 2412; RB: 3380; MV-F: 26933; MV-C: 54392.

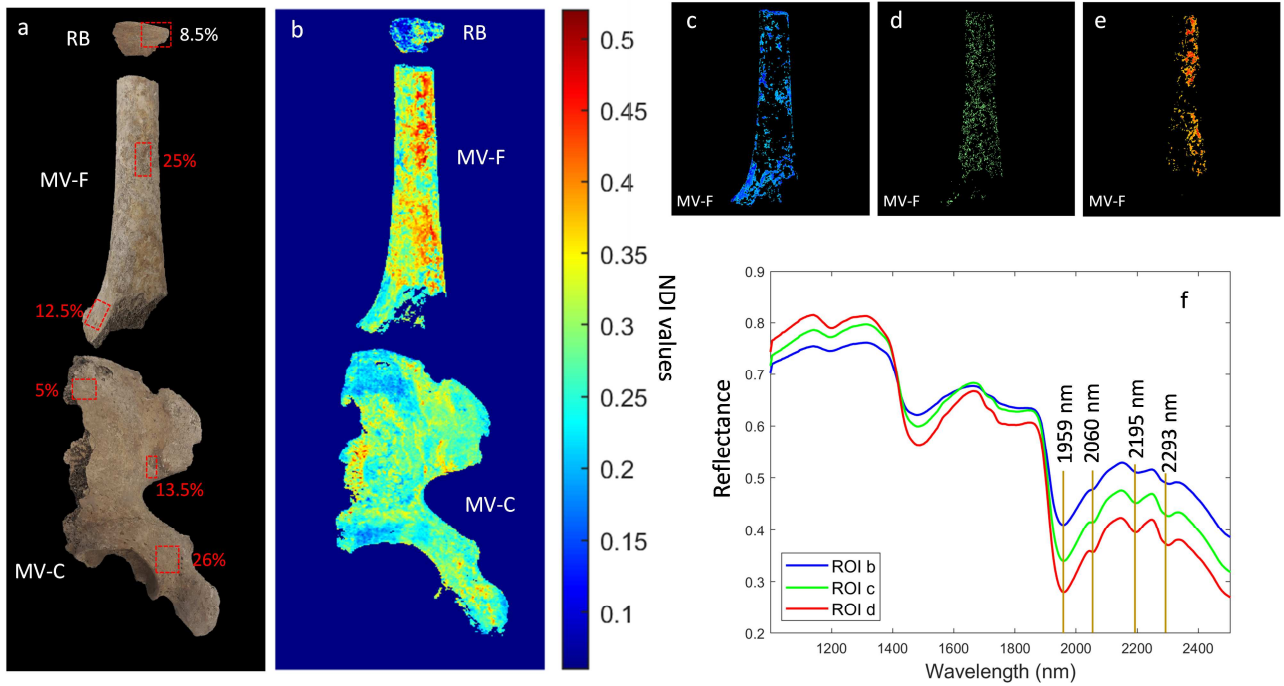
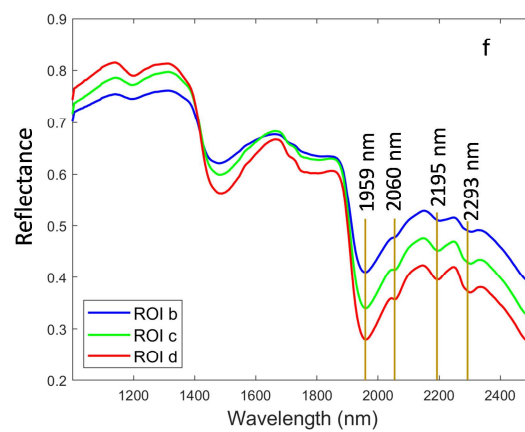
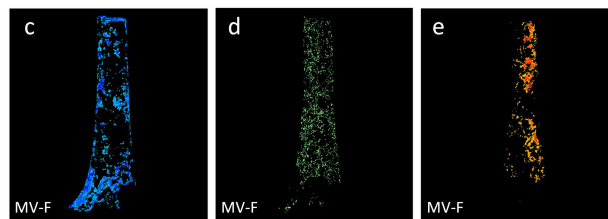
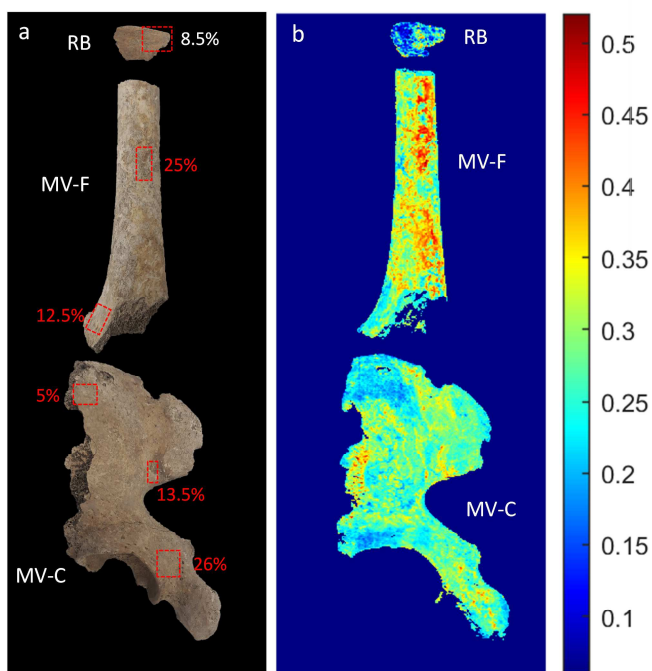


Figure 3. NIR-HSI results on test samples. a) Photographs of the test samples; sampling area for collagen extraction are reported (red rectangles); samples were submitted to the quantification of collagen through bone demineralization by HCl; for each investigated area the results are highlighted (% wt of collagen) and the subsample name is reported (see Table 1); b) NDI merged image of test samples (from the above): RB, MV-F, MV-C; c,d,e) ROIs referred to areas with different collagen content (blue: low, green: mid-level, red: high) in sample MV-F individually-scaled map; f) extracted averaged spectra from each ROI identified; diagnostic bands attributed to collagen (2060 nm: N-H stretching combination band; 2195 nm: N-H bending second overtone and C=O stretching combination 2293 nm: C-H stretching and bending combination band) and to hydroxyapatite (1959 nm: O-H banding second overtone and O-H stretching combination band) are marked in the plot.

Table 1. Information about the bone samples employed in this work. Collagen yields were calculated as the percentage of the extracted collagen weight over the total weight of the original bone sample after HCl demineralization.

Sample name	Bone sample type	Collagen yield (% wt)	Whole-bone median NDI value	Archaeological site	Approximate sample age	Reference
FB-A	Fauna	2.9	0.22	Savorgnano (Udine)	End of 7th century AD	-
FB-B	Fauna	2.9	0.23	Savorgnano (Udine)	End of 7th century AD	-
FB-C	Fauna	8	0.26	Savorgnano (Udine)	End of 7th century AD	-
FB-D	Fauna	8.5	0.26	Savorgnano (Udine)	End of 7th century AD	-
FB-E	Fauna	15	0.27	Savorgnano (Udine)	End of 7th century AD	-
FB-F	Fauna	20	0.29	Savorgnano (Udine)	End of 7th century AD	-
RB	Fauna	8.7	0.20	Riparo Broion (Vicenza, Italy)	45,000 years BP	(23)
MV-F1	Human	25	0.32	Monterenzio Vecchio (Bologna, Italy)	4th-3rd cent BC	(22)
MV-F2	Human	12.5	-	Monterenzio Vecchio (Bologna, Italy)	4th-3rd cent BC	(22)
MV-C1	Human	5.3	0.27	Monterenzio Vecchio (Bologna, Italy)	4th-3rd cent BC	(22)
MV-C2	Human	13.5	-	Monterenzio Vecchio (Bologna, Italy)	4th-3rd cent BC	(22)
MV-C3	Human	26.4	-	Monterenzio Vecchio (Bologna, Italy)	4th-3rd cent BC	(22)



Highlights

- Near-infrared hyperspectral imaging for localising collagen in ancient bones
- Computation of normalized difference images for high-throughput chemical mapping
- Relative estimation of collagen content within a sample and between samples
- Efficient non-destructive strategy to select sampling areas in entire specimens
- Green and rapid screening method which saves bones for further analyses